

Numerically Computing Finite Temperature Loop Integrals using pySecDec

D. Harnett*, Siyuan Li† and T.G. Steele‡

Department of Physics and Engineering Physics, University of Saskatchewan, Saskatoon, SK, S7N 5E2, Canada

January 11, 2024

Abstract

Finite-temperature quantum field theory provides the foundation for many important phenomena in the Standard Model and extensions, including phase transitions, baryogenesis, and gravitational waves. Methods are developed to enable application of pySecDec (a Python-language-based package designed for numerical calculation of dimensionally-regulated loop integrals) to numerically evaluate finite-temperature loop integrals in the imaginary time (Matsubara) formalism. These methods consist of two main elements: an inverse Wick rotation that converts a finite-temperature loop integral into a form applicable to pySecDec, and asymptotic techniques to regulate and accelerate convergence of the Matsubara frequency summations. Numerical pySecDec evaluation of finite-temperature, two-point and three-point, one-loop topologies for scalar fields is used to illustrate and validate these new methodologies. Advantages of these finite-temperature pySecDec numerical methods are illustrated by the inclusion of multiple mass and external momentum scales.

1 Introduction

Finite-temperature quantum field theory (see *e.g.*, Refs. [1–4] for reviews) provides the foundation for many important phenomena in the Standard Model and beyond. In particular, finite temperature effects in the effective potential for studying phase transitions (see *e.g.*, Refs. [5–8] for reviews, applications to the Standard Model [9, 10] and extensions [11, 12]) are an essential ingredient for studying baryogenesis (see *e.g.*, Refs. [7, 13] for reviews) and gravitational waves (see *e.g.*, Refs. [7, 8, 14] for reviews).

Finite-temperature quantum field theory in the imaginary time (Matsubara) formalism amounts to a simple modification of zero-temperature propagators, replacing the temporal component of each four-momentum with a discretized Matsubara frequency [15]. The additional energy scale associated with temperature leads to greater calculational challenges in evaluating loop integrals, particularly in models with multiple mass scales. It is therefore valuable to develop new methods for evaluating finite-temperature loop integrals to enable the study of increasingly elaborate extensions of the Standard Model.

The computational program pySecDec [16, 17] implements sector decomposition methods [18] to numerically calculate dimensionally-regularized integrals. pySecDec draws upon FORM [19–21], GSL [22],

*derek.harnett@shaw.ca

†siyuan.li@usask.ca

‡tom.steele@usask.ca

and the CUBA library [23, 24]. It has previously been demonstrated that pySecDec can be adapted to QCD sum-rule calculations at leading- and next-to-leading order [25, 26]. In this paper we develop methods to enable application of pySecDec to numerically evaluate finite-temperature loop integrals. One-loop bosonic two-point and three-point finite-temperature loop integrals (such as could emerge in scalar field theories) are used to develop and benchmark these new methodologies. As outlined below, two methodological elements are needed to apply pySecDec to finite-temperature loop integrals. The first methodological element is an inverse Wick rotation needed to convert a finite-temperature loop integral into a form applicable to pySecDec, and the second element is asymptotic techniques that accelerate or regulate the convergence of the sum over Matsubara frequencies.

In Section 2, three-point functions are first examined to establish the methodology in cases where the corresponding zero-temperature loop integral converges, but is overall complicated by the presence of multiple mass scales. Then, in Section 3, these methods are extended to the case where dimensional regularization is needed for the corresponding zero-temperature loop integral. A summary and discussion of the new pySecDec finite-temperature loop integration methodology is provided in Section 4.

2 The Finite-Temperature Three-Point Function

In the Matsubara formalism, the three-point vertex function for scalar fields in four spacetime dimensions at Euclidean external momenta $p_{1E} = (p_{1E}^0, \vec{p}_1)$ and $p_{2E} = (p_{2E}^0, \vec{p}_2)$ for propagator masses $\{m_i\}_{i=1}^3$ and finite inverse temperature $\beta = 1/T$ is given by (see *e.g.*, Ref. [1])

$$\Gamma_T(p_{1E}, p_{2E}) = \frac{1}{\beta} \sum_{n=-\infty}^{\infty} \int \frac{d^3k}{(2\pi)^3} \frac{1}{\left(\omega_n^2 + |\vec{k}|^2 + m_3^2\right) \left((\omega_n + p_{2E}^0)^2 + |\vec{k} + \vec{p}_2|^2 + m_1^2\right)} \times \frac{1}{\left((\omega_n - p_{1E}^0)^2 + |\vec{k} - \vec{p}_1|^2 + m_2^2\right)} \quad (1)$$

where

$$\omega_n = \frac{2n\pi}{\beta} \quad (2)$$

are the bosonic Matsubara frequencies (or energies) [15]. Note that p_{1E}^0 and p_{2E}^0 must also be Matsubara frequencies; the subscript ‘‘E’’ has been introduced for notational consistency between (1) and its zero-temperature limit (13) below. The Feynman diagram of the three-point vertex function Eq. (1) is shown in Fig. 1, where the external momenta can be interpreted as arising from either a single scalar field (*e.g.*, a ϕ^3 interaction) or multiple fields (*e.g.*, a ϕ^4 interaction). Defining the spatial integral

$$\mathcal{S}(\vec{p}_1, \vec{p}_2, \Delta_1, \Delta_2, \Delta_3) = \int \frac{d^3k}{(2\pi)^3} \frac{1}{\left(|\vec{k}|^2 + \Delta_3\right) \left(|\vec{k} + \vec{p}_2|^2 + \Delta_1\right) \left(|\vec{k} - \vec{p}_1|^2 + \Delta_2\right)} \quad (3)$$

lets us write (1) as

$$\Gamma_T(p_{1E}, p_{2E}) = \frac{1}{\beta} \sum_{n=-\infty}^{\infty} \mathcal{S}\left(\vec{p}_1, \vec{p}_2, \omega_n^2 + m_3^2, (\omega_n + p_{2E}^0)^2 + m_1^2, (\omega_n - p_{1E}^0)^2 + m_2^2\right). \quad (4)$$

Note that the spatial integral (3) converges as does the series in (4); thus, it is not necessary to use dimensional regularization in this (four-dimensional spacetime) case. Convergent or not, however, pySecDec can be used to efficiently numerically evaluate integrals like that of (3). Section 3 below presents an application for which dimensional regularization is necessary.

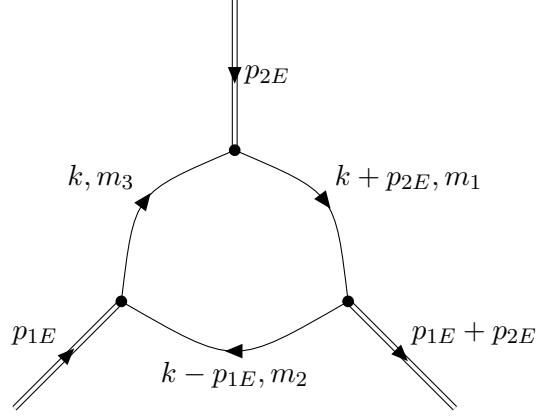


Figure 1: The 3-point function Feynman diagram where the double lines represent the total incoming momenta of the external fields within the model of interest (*e.g.*, single field for a ϕ^3 interaction or two fields for a ϕ^4 interaction).

To apply pySecDec to the spatial integral (3), for an arbitrary spatial momentum \vec{p} , we define a corresponding Minkowski \vec{p}_M by

$$p_M^1 = ip^1 \quad (5)$$

$$p_M^i = p^i \text{ for } i \neq 1. \quad (6)$$

The transformation (5)–(6) can be thought of as an inverse Wick rotation, but on the first spatial components rather than on the temporal components. Then, defining \mathcal{P} such that

$$\mathcal{S}(\vec{p}_1, \vec{p}_2, \Delta_1, \Delta_2, \Delta_3) = \mathcal{P}(\vec{p}_{1M}, \vec{p}_{2M}, \Delta_1, \Delta_2, \Delta_3) \quad (7)$$

gives

$$\begin{aligned} \mathcal{P}(\vec{p}_{1M}, \vec{p}_{2M}, \Delta_1, \Delta_2, \Delta_3) = i \int \frac{d^3 k_M}{(2\pi)^3} & \frac{1}{(\vec{k}_M \cdot \vec{k}_M - \Delta_3 + i0^+) \left((\vec{k}_M + \vec{p}_{2M}) \cdot (\vec{k}_M + \vec{p}_{2M}) - \Delta_1 + i0^+ \right)} \\ & \times \frac{1}{\left((\vec{k}_M - \vec{p}_{1M}) \cdot (\vec{k}_M - \vec{p}_{1M}) - \Delta_2 + i0^+ \right)} \quad (8) \end{aligned}$$

where we have used (3) and (5)–(7). Throughout, we use the notation $\vec{u}_M \cdot \vec{v}_M$ to denote a Minkowski dot product of three-component vectors \vec{u}_M, \vec{v}_M , *e.g.*,

$$\vec{k}_M \cdot \vec{k}_M = (k_M^1)^2 - (k^2)^2 - (k^3)^2. \quad (9)$$

Note that the usual $i0^+$ limit within the propagators ensures that a Wick rotation of (8) in the first spatial components leads to (7), and hence Eqs. (5)–(6) constitute an inverse Wick rotation. The right-hand side of (8) has the form of a three-dimensional spacetime integral of a product of Minkowski-space propagators and, as such, is in a form suitable for numerical evaluation using pySecDec. Then, with

$$\Delta_1 = \omega_n^2 + m_3^2 \quad (10)$$

$$\Delta_2 = (\omega_n + p_{2E}^0)^2 + m_1^2 \quad (11)$$

$$\Delta_3 = (\omega_n - p_{1E}^0)^2 + m_2^2 \quad (12)$$

in (7)–(8), we can calculate $\Gamma_T(p_{1E}, p_{2E})$ using (4). Thus, the inverse Wick rotation as represented in Eqs. (5)–(6) and employed in (7)–(8) is the first methodological element needed to evaluate finite-temperature loop integrals with pySecDec.

The zero-temperature limit (*i.e.*, $\beta \rightarrow \infty$) of (1) is given by

$$\Gamma_0(p_{1E}, p_{2E}) = \int \frac{d^4 k_E}{(2\pi)^4} \frac{1}{(k_E^2 + m_3^2) ((k_E + p_{2E})^2 + m_1^2) ((k_E - p_{1E})^2 + m_2^2)} \quad (13)$$

where

$$k_E^2 = (k_E^0)^2 + |\vec{k}|^2 = (k_E^0)^2 + (k^1)^2 + (k^2)^2 + (k^3)^2 \quad (14)$$

with analogous expressions for $(k_E + p_{2E})^2$ and $(k_E - p_{1E})^2$. Alternatively, Γ_0 can be expressed in terms of Minkowski momenta by defining Λ_0 through

$$\Gamma_0(p_{1E}, p_{2E}) = \Lambda_0(p_1, p_2) \quad (15)$$

which gives

$$\Lambda_0(p_1, p_2) = i \int \frac{d^4 k}{(2\pi)^4} \frac{1}{(k^2 - m_3^2 + i0^+) ((k + p_2)^2 - m_1^2 + i0^+) ((k - p_1)^2 - m_2^2 + i0^+)} \quad (16)$$

where

$$k^0 = ik_E^0, \quad p_1^0 = ip_{1E}^0, \quad p_2^0 = ip_{2E}^0 \quad (17)$$

(note that spatial components are unaffected by such Wick rotations on temporal components) and where

$$k^2 = (k^0)^2 - |\vec{k}|^2 = (k^0)^2 - (k^1)^2 - (k^2)^2 - (k^3)^2 \quad (18)$$

with analogous expressions for $(k + p_2)^2$ and $(k - p_1)^2$. Equations (15)–(18) again represent an inverse Wick rotation. The right-hand side of (16) is in a form suitable for numerical evaluation using pySecDec because the $i0^+$ limit corresponds to standard Minkowski-space propagators.

As an aside, we note that (13) can be written in terms of the spatial integral (3) as

$$\Gamma_0(p_{1E}, p_{2E}) = \int_{-\infty}^{\infty} \frac{dk_E^0}{2\pi} \mathcal{S}(\vec{p}_1, \vec{p}_2, (k_E^0)^2 + m_3^2, (k_E^0 + p_{2E}^0)^2 + m_1^2, (k_E^0 - p_{1E}^0)^2 + m_2^2). \quad (19)$$

In (19), the integrand \mathcal{S} can be numerically evaluated with pySecDec using (7)–(8) for $\Delta_1 = m_1^2$, $\Delta_2 = m_2^2$, and $\Delta_3 = m_3^2$ while the outside integral over k_E^0 can be numerically evaluated using a variety of one-dimensional techniques. Comparing Γ_0 as calculated using (15)–(16), a straightforward application of pySecDec to the entire spacetime integral, and (19) serves as a valuable consistency check on the inverse Wick rotation methodology (5)–(8) and the implementation of (3).

To identify the scaling behaviour of Γ_T and Γ_0 , we re-express both in terms of dimensionless quantities. In (1), we introduce a dimensionless integration variable $\vec{\kappa}$,

$$\vec{\kappa} = \frac{\beta}{2\pi} \vec{k} \implies d^3 \kappa = \left(\frac{\beta}{2\pi} \right)^3 d^3 k. \quad (20)$$

Similarly, we define dimensionless variables ℓ_1 , \vec{q}_1 , ℓ_2 , and \vec{q}_2 ,

$$\ell_i = \frac{\beta}{2\pi} p_{iE}^0, \quad \vec{q}_i = \frac{\beta}{2\pi} \vec{p}_i \quad \text{for } i \in \{1, 2\}, \quad (21)$$

where ℓ_1 and ℓ_2 must be integers because p_{1E}^0 and p_{2E}^0 are Matsubara frequencies. With

$$M = \max\{m_i\}_{i=1}^3, \quad (22)$$

we define dimensionless mass parameters ξ_i ,

$$\xi_i = \frac{m_i}{M}. \quad (23)$$

Then, we define $\tilde{\Gamma}_T$ through

$$\Gamma_T(p_{1E}, p_{2E}) = \frac{1}{M^2} \tilde{\Gamma}_T(\ell_1, \vec{q}_1; \ell_2, \vec{q}_2). \quad (24)$$

Substituting (20)–(23) into (1), we find, using (24),

$$\begin{aligned} \tilde{\Gamma}_T(\ell_1, \vec{q}_1; \ell_2, \vec{q}_2) &= \frac{a^2}{2\pi} \sum_{n=-\infty}^{\infty} \int \frac{d^3\kappa}{(2\pi)^3} \frac{1}{(n^2 + |\vec{\kappa}|^2 + a^2\xi_3^2) \left((n + \ell_2)^2 + |\vec{\kappa} + \vec{q}_2|^2 + a^2\xi_1^2 \right)} \\ &\quad \times \frac{1}{\left((n - \ell_1)^2 + |\vec{\kappa} - \vec{q}_1|^2 + a^2\xi_2^2 \right)} \end{aligned} \quad (25)$$

where

$$a = \frac{\beta M}{2\pi} \quad (26)$$

is dimensionless. Therefore, $\tilde{\Gamma}_T$ is also dimensionless.

Next for Γ_0 , in (13), we apply the change of variables

$$\kappa_E = \frac{k_E}{M} \implies d^4\kappa_E = \frac{1}{M^4} d^4k_E \quad (27)$$

where M is defined in (22). Analogous to (24), we define $\tilde{\Gamma}_0$ through

$$\Gamma_0(p_{1E}, p_{2E}) = \frac{1}{M^2} \tilde{\Gamma}_0(\ell_1, \vec{q}_1; \ell_2, \vec{q}_2) \quad (28)$$

where ℓ_i and \vec{q}_i are defined in (21). Substituting (21), (23), and (27) into (13), we find, using (28),

$$\begin{aligned} \tilde{\Gamma}_0(\ell_1, \vec{q}_1; \ell_2, \vec{q}_2) &= \int \frac{d^4\kappa_E}{(2\pi)^4} \frac{1}{\left[(\kappa_E^0)^2 + |\vec{\kappa}|^2 + \xi_3^2 \right] \left[\left(\kappa_E^0 + \frac{\ell_2}{a} \right)^2 + \left| \vec{\kappa} + \frac{\vec{q}_2}{a} \right|^2 + \xi_1^2 \right]} \\ &\quad \times \frac{1}{\left[\left(\kappa_E^0 - \frac{\ell_1}{a} \right)^2 + \left| \vec{\kappa} - \frac{\vec{q}_1}{a} \right|^2 + \xi_2^2 \right]} \end{aligned} \quad (29)$$

which shows that $\tilde{\Gamma}_0$ is dimensionless. Strictly speaking, in (28)–(29), ℓ_1 and ℓ_2 need not be integers. Also note that (29) can be put into a Euclidean four-dimensional covariant form by associating ℓ_i/a and \vec{q}_i/a for each i with the temporal and spatial components respectively of a four-dimensional Euclidean vector.

The inverse Wick rotation methodology introduced above can be applied in a straightforward way to the rescaled integrals (24) and (25). It is also important to emphasize that pySecDec requires input of numeric values for all parameters within the loop integrals, and hence (apart from the scaling arguments), the masses m_i , inverse temperature β , and external momenta $p_{1E} = (p_{1E}^0, \vec{p}_1)$ and $p_{2E} = (p_{2E}^0, \vec{p}_2)$ are needed as numeric inputs to pySecDec.

In computing $\tilde{\Gamma}_T$, we generally need to truncate the series outside of $n \in \{-n_{\max}, -n_{\max} + 1, \dots, n_{\max}\}$ for some n_{\max} . We can, however, estimate the size of the corresponding truncation

error. Suppressing function arguments, we write

$$\tilde{\Gamma}_T = \sum_{n=-\infty}^{\infty} \tilde{\Gamma}_{T,n} \quad (30)$$

$$= \sum_{n=-n_{\max}}^{n_{\max}} \tilde{\Gamma}_{T,n} + \sum_{n=n_{\max}+1}^{\infty} \tilde{\Gamma}_{T,n} + \sum_{n=-\infty}^{-(n_{\max}+1)} \tilde{\Gamma}_{T,n} \quad (31)$$

where, from (25) and (30),

$$\tilde{\Gamma}_{T,n} = \frac{a^2}{2\pi} \int \frac{d^3\kappa}{(2\pi)^3} \frac{1}{(n^2 + |\vec{\kappa}|^2 + a^2\xi_3^2) \left((n + \ell_2)^2 + |\vec{\kappa} + \vec{q}_2|^2 + a^2\xi_1^2 \right)} \times \frac{1}{\left((n - \ell_1)^2 + |\vec{\kappa} - \vec{q}_1|^2 + a^2\xi_2^2 \right)}. \quad (32)$$

If n_{\max} is chosen large enough such that $|n| > n_{\max}$ implies that $|n| \gg a\xi_i$, $|n| \gg |\ell_i|$, and $|n| \gg |\vec{q}_i|$, then

$$\begin{aligned} \tilde{\Gamma}_T &\approx \sum_{n=-n_{\max}}^{n_{\max}} \tilde{\Gamma}_{T,n} + 2 \sum_{n=n_{\max}+1}^{\infty} \frac{a^2}{2\pi} \int \frac{d^3\kappa}{(2\pi)^3} \frac{1}{(n^2 + |\vec{\kappa}|^2)^3} \\ &= \sum_{n=-n_{\max}}^{n_{\max}} \tilde{\Gamma}_{T,n} + \frac{a^2}{32\pi^2} \sum_{n=n_{\max}+1}^{\infty} \frac{1}{n^3} \\ &= \sum_{n=-n_{\max}}^{n_{\max}} \tilde{\Gamma}_{T,n} + \frac{a^2}{32\pi^2} \left(\zeta(3) - \sum_{n=1}^{n_{\max}} \frac{1}{n^3} \right) \\ \implies \tilde{\Gamma}_T &\approx \sum_{n=-n_{\max}}^{n_{\max}} \tilde{\Gamma}_{T,n} + \frac{a^2}{32\pi^2} \zeta[3, n_{\max} + 1] \end{aligned} \quad (33)$$

where $\zeta[s, b]$ is the generalized Riemann zeta function

$$\zeta[s, b] = \sum_{k=0}^{\infty} \frac{1}{(k+b)^s}. \quad (34)$$

Accordingly, we refer to the final term on the right-hand side of (33) as the zeta-function correction. In general, including zeta-function corrections in calculations of $\tilde{\Gamma}_T$ allows for a significantly lower value of n_{\max} to be used which speeds up computation times considerably. This is illustrated in Figure 2 where we plot (33) with and without the zeta-function correction for various values of a . The corrected versions converge more quickly than the uncorrected, and, hence, use of the large- n asymptotic form of the finite-temperature loop integrals accelerates convergence of the Matsubara frequency summation. This asymptotic technique is the second element of our pySecDec methodology for finite-temperature loop integrals. In Section 3, asymptotic techniques are needed to regulate the Matsubara sum in addition to accelerating convergence. All calculations of $\tilde{\Gamma}_T$ in the rest of this section include the zeta-correction.

To conclude this section, we show some plots of the dimensionless, zero-temperature vertex function $\tilde{\Gamma}_0$ (recall (28)–(29)) and the dimensionless, vertex function finite-temperature correction $\tilde{\Gamma}_T - \tilde{\Gamma}_0$ (recall (24)–(25)), both calculated using pySecDec. In Figure 3, we show $\tilde{\Gamma}_0$ as a function of a for several values of $\ell = \ell_1 = \ell_2$. In obtaining Figure 3, it has been verified that the two approaches of (15)–(16) and (19) are identical, providing a robust self-consistency check on our methodology. In

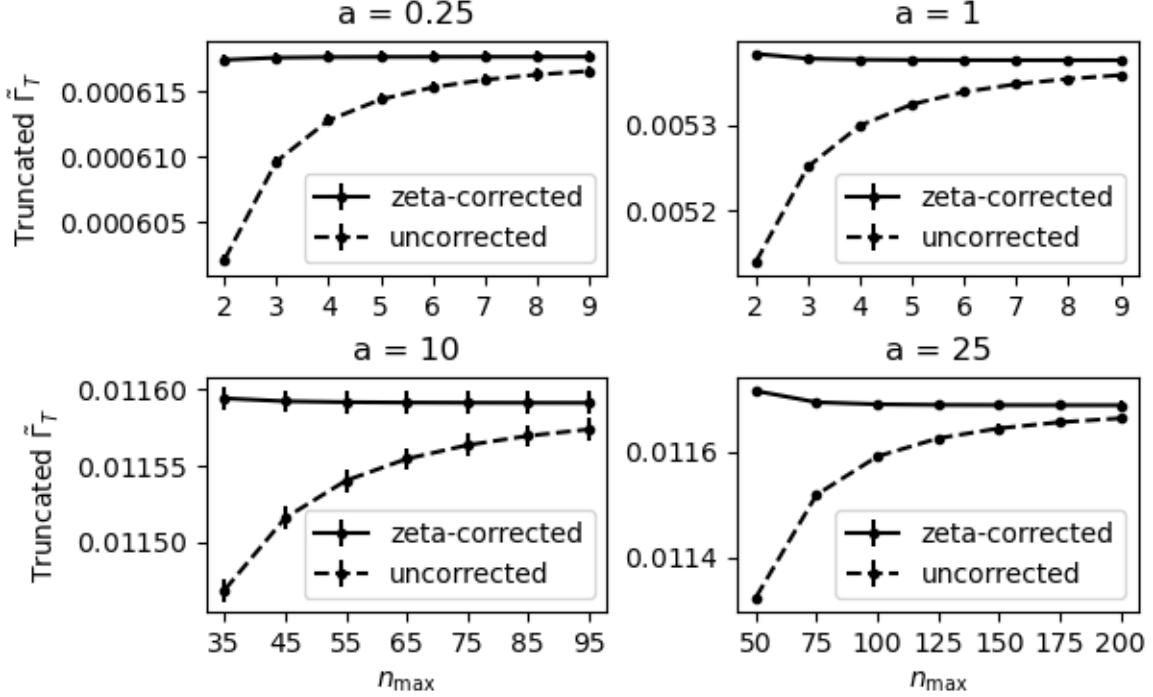


Figure 2: The right-hand side of (33) with and without the zeta-function correction versus n_{\max} for $\ell_1 = \ell_2 = 1$, $\vec{q}_1 = \vec{q}_2 = 0$, $\xi_1 = 1$, $\xi_2 = 0.5$, and $\xi_3 = 0$ at various values of a .

Figure 4, we show $\tilde{\Gamma}_T - \tilde{\Gamma}_0$ as a function of a for the same values of ℓ . In Figure 5, we show $\tilde{\Gamma}_0$ as a function of q^1 where $\vec{q}_1 = \vec{q}_2 = (q^1, 0, 0)$ for several values of a . In Figure 6, we show $\tilde{\Gamma}_T - \tilde{\Gamma}_0$ as a function of q^1 for the same values of a . In obtaining Figures 2–6 we have compared the pySecDec numerical results with an analytic calculation that is possible in the limiting case $\xi_2 = \xi_3 = 1$ and $\vec{q}_1 = \vec{q}_2 = 0$. Within the remaining $\{a, \ell_1, \ell_2\}$ -parameter space, the difference between the analytic and pySecDec numerical results are smaller than the pySecDec-provided numerical errors, providing a validation of the methodology. The advantages and adaptability of our finite numerical pySecDec methodology are illustrated by the incredible diversity of physical scales (mass, temperature, momentum) encompassed by Figures 3–6.

3 The Finite-Temperature Two-Point Function

In this Section, we consider a case where dimensional regularization is needed within the finite-temperature loop integrals, which has implications for the Matsubara frequency summation.

Similar to the three-point function (1), the Matsubara formalism provides an expression for the two-point function in four spacetime dimensions with propagator masses $\{m_i\}_{i=1}^2$ at Euclidean external momentum $p_E = (p_E^0, \vec{p})$ (as in Section 2, the subscript “E” is used for notational consistency between (35) and its zero-temperature limit (38) below) and finite inverse temperature $\beta = 1/T$ (see *e.g.*, Ref. [1]):

$$\Pi_T(p_E) = \frac{1}{2\beta} \sum_{n=-\infty}^{\infty} \int \frac{d^3k}{(2\pi)^3} \frac{1}{(\omega_n^2 + |\vec{k}|^2 + m_1^2) ((\omega_n + p_E^0)^2 + |\vec{k} + \vec{p}|^2 + m_2^2)} \quad (35)$$

where ω_n , the (bosonic) Matsubara frequencies (or energies) [15], are defined in (2) and where (35) contains a diagrammatic symmetry factor of $\frac{1}{2}$. Note that p_E^0 must be a Matsubara energy. The

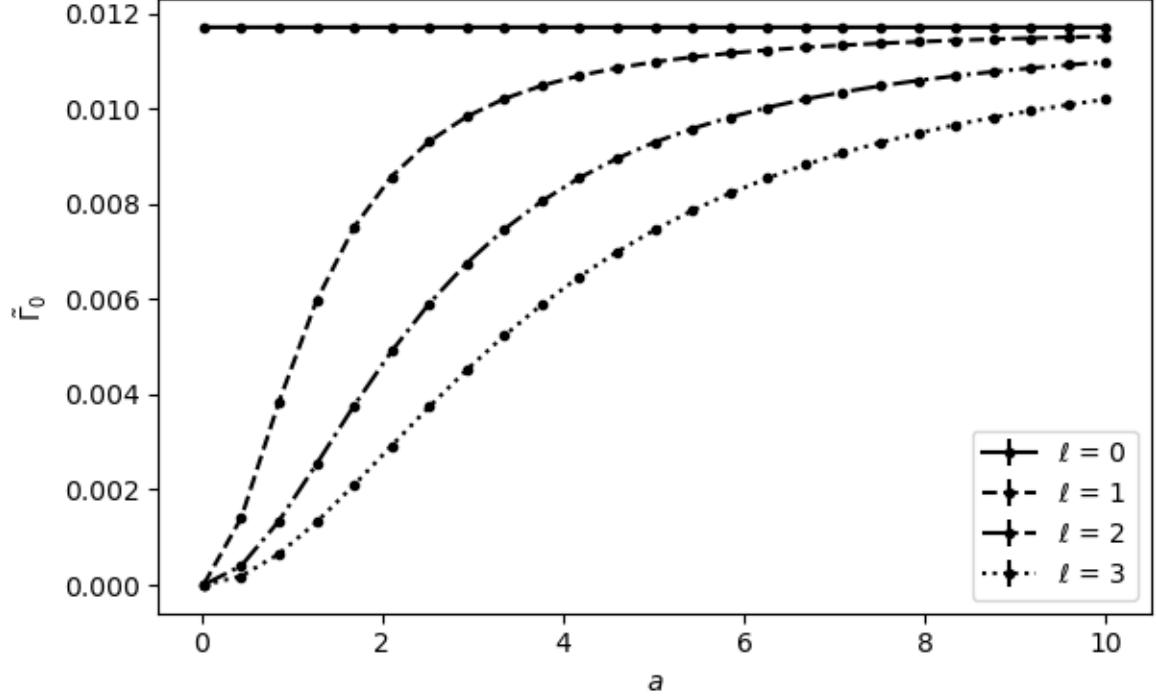


Figure 3: The dimensionless, zero-temperature vertex function $\tilde{\Gamma}_0$ versus a for $\vec{q}_1 = \vec{q}_2 = 0$, $\xi_1 = 1$, $\xi_2 = 0.5$, and $\xi_3 = 0$ at various values of $\ell = \ell_1 = \ell_2$. Error bars reflecting the numerical uncertainty as determined by pySecDec are not visible.

Feynman diagram corresponding to (35) is shown in Figure 7 where, again, the external momentum can be interpreted as arising from either a single scalar field (*e.g.*, a ϕ^3 interaction) or multiple fields, *e.g.*, a ϕ^4 interaction). In anticipation of the need to use dimensional regularization in $D = 4 - 2\epsilon$ spacetime dimensions, we define the spatial integral

$$I(\vec{p}, \Delta_1, \Delta_2) = \frac{\nu^{2\epsilon}}{2\beta} \int \frac{d^{D-1}k}{(2\pi)^{D-1}} \frac{1}{\left(|\vec{k}|^2 + \Delta_1\right) \left(|\vec{k} + \vec{p}|^2 + \Delta_2\right)} \quad (36)$$

where ν is the renormalization scale. [Unlike in (3), here, we absorb a factor of β^{-1} into the definition of the spatial integral (36).] Using (36) lets us express (35) as

$$\Pi_T(p_E) = \sum_{n=-\infty}^{\infty} I(\vec{p}, \omega_n^2 + m_1^2, (\omega_n + p_E^0)^2 + m_2^2). \quad (37)$$

Similarly, the dimensionally-regularized, zero-temperature ($\beta \rightarrow \infty$) two-point function is given by

$$\Pi_0(p_E) = \frac{\nu^{2\epsilon}}{2} \int \frac{d^D k_E}{(2\pi)^D} \frac{1}{(k_E^2 + m_1^2) ((k_E + p_E)^2 + m_2^2)} \quad (38)$$

or, in terms of Minkowski momenta, by

$$\Pi_0(p) = -i \frac{\nu^{2\epsilon}}{2} \int \frac{d^D k}{(2\pi)^D} \frac{1}{(k^2 - m_1^2 + i0^+) ((k+p)^2 - m_2^2 + i0^+)}, \quad (39)$$

where p_E^0 and p^0 as well as k_E^0 and k^0 are related as in (17). Throughout this section, we denote the two-point, bosonic correlator as Π regardless of the particular choice of function argument(s) such as p_E in (38) or p in (39).

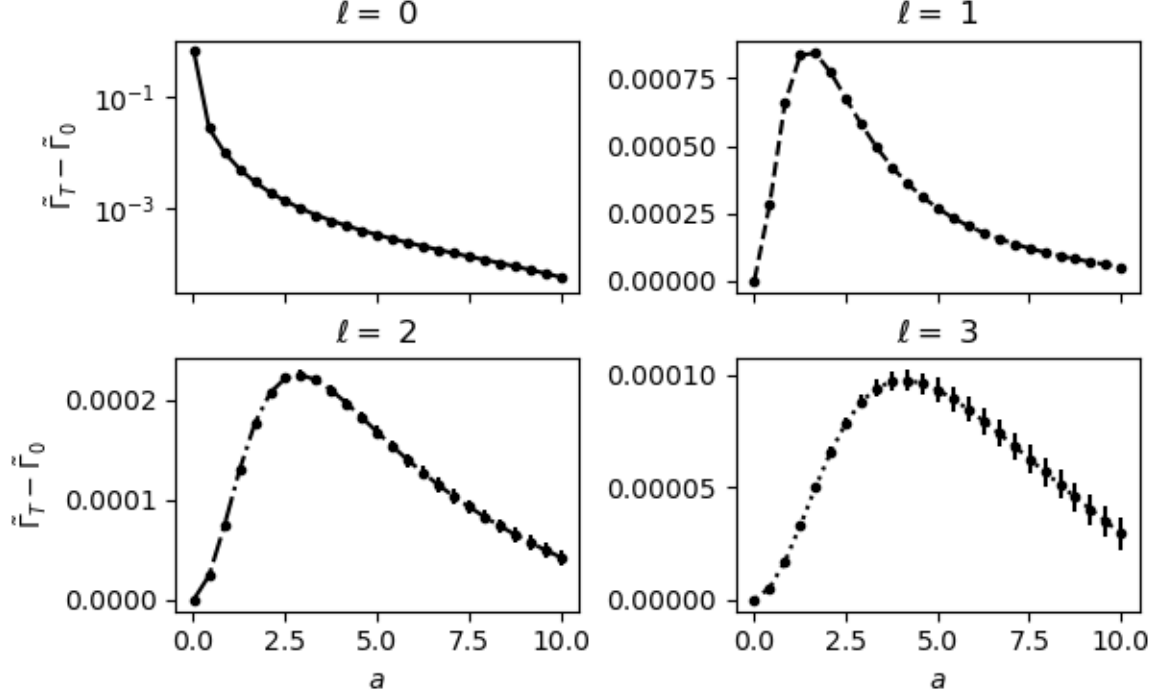


Figure 4: The dimensionless, finite-temperature vertex function correction $\tilde{\Gamma}_T - \tilde{\Gamma}_0$ versus a for $\vec{q}_1 = \vec{q}_2 = 0$, $\xi_1 = 1$, $\xi_2 = 0.5$, and $\xi_3 = 0$ at various values of $\ell = \ell_1 = \ell_2$. Note that the vertical-axis scale of the $\ell = 0$ plot is logarithmic whereas the others are linear. Error bars (where visible) reflect the numerical uncertainty as determined by pySecDec.

Compared to the three-point function, calculation of the two-point function is complicated by the fact that both (35) and (38) diverge in four spacetime dimensions. To see explicitly how the divergence in (35) arises and can be dimensionally-regularized, we consider the large- $|n|$ limit of (36) with $\Delta_1 = \omega_n^2 + m_1^2$ and $\Delta_2 = (\omega_n + p_E^0)^2 + m_2^2$ where ω_n is large in magnitude compared to the masses m_1 , m_2 and all components of the external momentum p_E . Then,

$$I(\vec{p}, \omega_n^2 + m_1^2, (\omega_n + p_E^0)^2 + m_2^2) \approx \frac{\nu^{2\epsilon}}{2\beta} \int \frac{d^{D-1}k}{(2\pi)^{D-1}} \frac{1}{(|\vec{k}|^2 + \omega_n^2)^2}. \quad (40)$$

Using standard dimensional-regularization results (see *e.g.*, Refs. [2, 27]) we can rewrite (40) as

$$I(\vec{p}, \omega_n^2 + m_1^2, (\omega_n + p_E^0)^2 + m_2^2) \approx \frac{1}{32\pi^2} \left[1 + \epsilon \left(\log \left(\frac{\beta^2 \nu^2}{4\pi^2} \right) - \gamma_E \right) \right] \frac{1}{(n^2)^{\frac{1}{2} + \epsilon}}. \quad (41)$$

Analogous to (30), we write

$$\Pi_T = \sum_{n=-\infty}^{\infty} \Pi_{T,n}, \quad (42)$$

$$\Pi_{T,n} = I(\vec{p}, \omega_n^2 + m_1^2, (\omega_n + p_E^0)^2 + m_2^2), \quad (43)$$

where, from (37) and (41), we have for large $|n|$

$$\Pi_{T,n} \approx \frac{1}{32\pi^2} \left[1 + \epsilon \left(\log \left(\frac{\beta^2 \nu^2}{4\pi^2} \right) - \gamma_E \right) \right] \frac{1}{|n|^{1+2\epsilon}}. \quad (44)$$

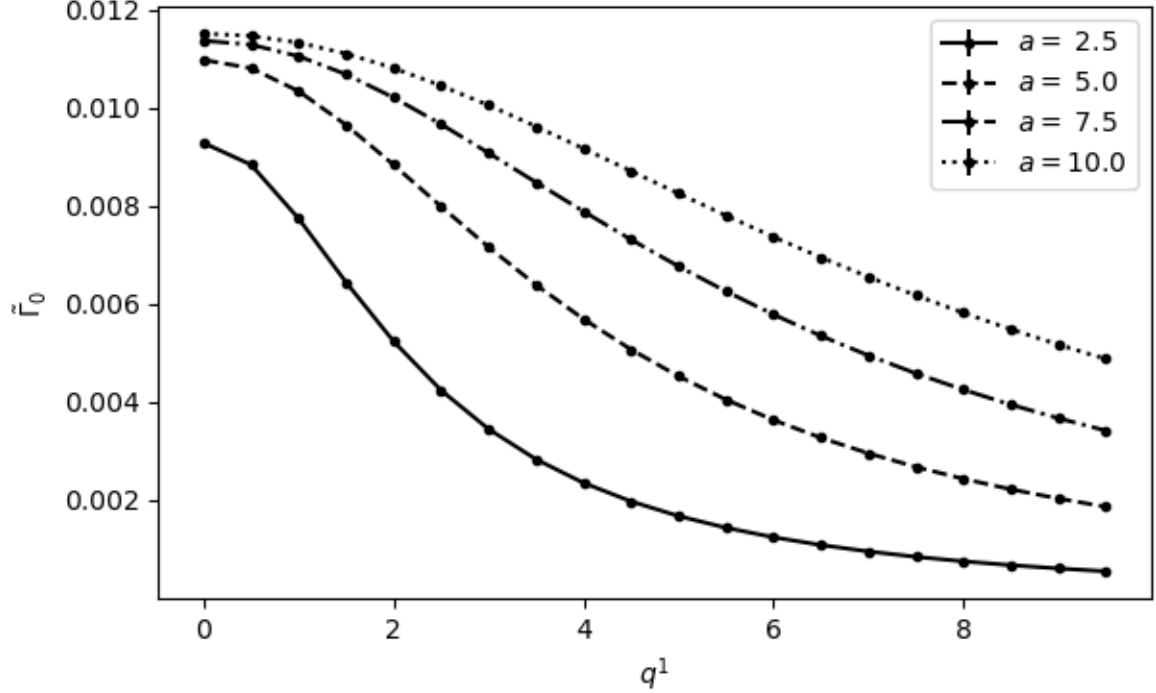


Figure 5: The dimensionless, zero-temperature vertex function $\tilde{\Gamma}_0$ versus q^1 for $\ell_1 = \ell_2 = 1$, $\xi_1 = 1$, $\xi_2 = 0.5$, and $\xi_3 = 0$ at various values of a . Error bars reflecting the numerical uncertainty as determined by pySecDec are not visible.

In the $\epsilon \rightarrow 0$ limit, we see from (42) and (44) that Π_T is divergent. However, dimensional regularization does parameterize this divergence via the zeta function. As for the three-point function, this regularization is achieved by truncating the exact series (42) and replacing it with the large n form (44) for $|n| > n_{\max}$

$$\begin{aligned} \Pi_T &\approx \sum_{n=-(n_{\max}-1)}^{n_{\max}-1} \Pi_{T,n} + \frac{1}{16\pi^2} \left[1 + \epsilon \left(\log \left(\frac{\beta^2 \nu^2}{4\pi} \right) - \gamma_E \right) \right] \sum_{n=n_{\max}}^{\infty} \frac{1}{n^{1+2\epsilon}} \\ &= \sum_{n=-(n_{\max}-1)}^{n_{\max}-1} \Pi_{T,n} + \frac{1}{16\pi^2} \left[1 + \epsilon \left(\log \left(\frac{\beta^2 \nu^2}{4\pi} \right) - \gamma_E \right) \right] \zeta[1 + 2\epsilon, n_{\max}]. \end{aligned} \quad (45)$$

Using the result

$$\zeta[1 + 2\epsilon, n_{\max}] = \frac{1}{2\epsilon} - \psi[n_{\max}] + \mathcal{O}(\epsilon), \quad (46)$$

where $\psi(z)$ is the digamma function, leads to a dimensionally-regularized (divergent) expression for Π_T

$$\Pi_T \approx \sum_{n=-(n_{\max}-1)}^{n_{\max}-1} \Pi_{T,n} - \frac{1}{16\pi^2} \psi[n_{\max}] + \frac{1}{32\pi^2} \left[\frac{1}{\epsilon} - \gamma_E + \log \left(\frac{\beta^2 \nu^2}{4\pi} \right) \right], \quad (47)$$

where irrelevant terms of $\mathcal{O}(\epsilon)$ are omitted and the approximation can be improved by increasing n_{\max} so that (41) becomes more accurate.

Although Π_T and Π_0 separately diverge, their difference, *i.e.*, the finite-temperature correction Π_s ,

$$\Pi_s = \Pi_T - \Pi_0 \quad (48)$$

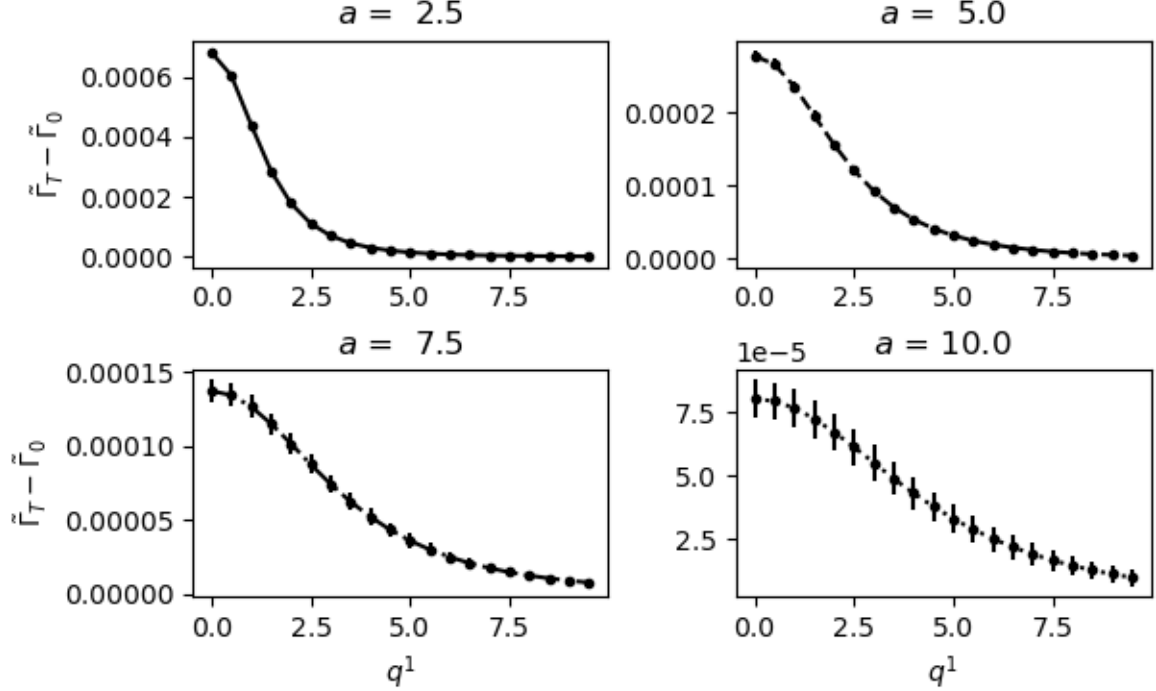


Figure 6: The dimensionless, finite-temperature vertex function correction $\tilde{\Gamma}_T - \tilde{\Gamma}_0$ versus q^1 for $\ell_1 = \ell_2 = 1$, $\xi_1 = 1$, $\xi_2 = 0.5$, and $\xi_3 = 0$ at various values of a . Error bars (where visible) reflect the numerical uncertainty as determined by pySecDec.

is finite. This behaviour is expected in mass-independent regularization schemes like dimensional regularization. As shown in (47), the divergence in Π_T comes from a series in n whereas the divergence in Π_0 comes from an integral over k_E (recall (38)). We can show analytically that these two divergences cancel in Π_s defined by (48). Expressing (38) in terms of the dimensionless integration variable $\kappa_E = k_E/M$ gives

$$\Pi_0(p_E) = \left(\frac{\nu^2}{M^2}\right)^\epsilon \frac{1}{2} \int \frac{d^D \kappa_E}{(2\pi)^D} \frac{1}{(\kappa_E^2 + \xi_1^2)((\kappa_E + q_E)^2 + \xi_2^2)}, \quad (49)$$

$$M = \max\{m_i\}_{i=1}^2, \quad \xi_i = \frac{m_i}{M}, \quad q_E = \frac{p_E}{M}, \quad q_E^0 = \frac{\ell}{a} \quad (50)$$

where a is defined in (26) and ℓ is the integer corresponding to the Matsubara energy $p_E^0 = 2\pi\ell/\beta$. Standard dimensional regularization methods (see *e.g.*, Ref. [27]) result in a divergence that is independent of p_E and the parameters ξ_i

$$\Pi_0(p_E) = \frac{1}{32\pi^2} \left[\frac{1}{\epsilon} - \gamma_E + \log(4\pi) - \log\left(\frac{M^2}{\nu^2}\right) \right] + f_0^{\text{finite}}(q_E, \xi_i) \quad (51)$$

where f_0^{finite} contains the remaining finite parts of Π_0 . Having analytically extracted the divergences from both Π_T and Π_0 , we have shown explicitly that they are equal and, as expected, temperature-independent. Thus the divergences cancel from the finite-temperature correction (48) leading to the the result

$$\Pi_s = \sum_{n=-(n_{\max}-1)}^{n_{\max}-1} \Pi_{T,n} - \frac{1}{16\pi^2} \psi[n_{\max}] + \frac{1}{16\pi^2} \log\left(\frac{a}{2}\right) - f_0^{\text{finite}}(q_E, \xi_i). \quad (52)$$

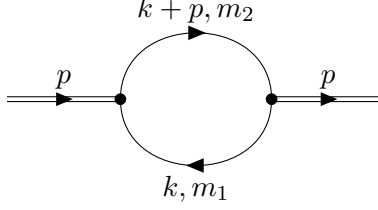


Figure 7: The 2-point function Feynman diagram where the double lines represent the total incoming momenta of the external fields within the model of interest (*e.g.*, a single field for a ϕ^3 interaction or two fields for a ϕ^4 interaction).

Because the divergent parts cancel in Π_s , the renormalization scale also cancels in (52) along with the usual dimensional-regularization terms γ_E and $\log(4\pi)$. Thus, to apply pySecDec to (52), we use $\Pi_{T,n}$ as calculated in pySecDec, and extract only the finite part of Π_0 from the pySecDec calculation to give a slightly modified version of (52) suited to pySecDec,

$$\Pi_s = \sum_{n=-(n_{\max}-1)}^{n_{\max}-1} \Pi_{T,n} - \frac{1}{16\pi^2} \psi[n_{\max}] + \frac{1}{16\pi^2} \log\left(\frac{a}{2}\right) + \frac{1}{32\pi^2} [-\gamma_E + \log(4\pi)] - \tilde{\Pi}_0^{\text{finite}}(q_E, \xi_i), \quad (53)$$

where $\tilde{\Pi}_0^{\text{finite}}$ is the finite part of the dimensionless integral (50) omitting the ν^2/M^2 renormalization-scale pre-factor

$$\tilde{\Pi}_0(q_E, \xi_i) = \frac{1}{2} \int \frac{d^D \kappa_E}{(2\pi)^D} \frac{1}{(\kappa_E^2 + \xi_1^2) ((k_E + q_E)^2 + \xi_2^2)}. \quad (54)$$

Note that the γ_E and $\log(4\pi)$ terms have been restored in (53) because they cannot easily be separated out from the pySecDec finite part. As an important numerical benchmark, the divergent part of Π_0 should be calculated in pySecDec to verify the $1/(32\pi^2\epsilon)$ -dependence in (51). The only remaining task is to develop a version of $\Pi_{T,n}$ suited to pySecDec.

As for the three-point function, we switch to dimensionless parameters. Based on our analytic result, we can anticipate the finiteness of (36) within dimensional regularization in $D = 4 - 2\epsilon$ space-time dimensions. Also, in $\Pi_{T,n}$, we can set $\epsilon = 0$, introduce dimensionless $\vec{\kappa}$ as in (20), and define dimensionless quantities ℓ , \vec{q} , and a as follows:

$$\ell = \frac{\beta}{2\pi} p_E^0, \quad \vec{q} = \frac{\beta}{2\pi} \vec{p}, \quad (55)$$

where a is defined in (26) and ℓ is an integer because p_E^0 is a Matsubara energy. Then,

$$\Pi_{T,n}(\{\ell, \vec{q}\}) = \frac{1}{4\pi} \int \frac{d^3 \kappa}{(2\pi)^3} \frac{1}{(n^2 + |\vec{\kappa}|^2 + \xi_1 a^2) \left((n + \ell)^2 + |\vec{\kappa} + \vec{q}|^2 + \xi_2 a^2 \right)}. \quad (56)$$

For $\Pi_{T,n}$, we implement an inverse Wick rotation much as we did when calculating the finite-temperature three-point function. Following (5), we define κ_M^1 and q_M^1 as

$$\kappa^1 = -i\kappa_M^1, \quad q^1 = -iq_M^1. \quad (57)$$

Then,

$$\Pi_{T,n}(\{\ell, \vec{q}_M\}) = \frac{-i}{4\pi} \int \frac{d^3 \kappa_M}{(2\pi)^3} \frac{1}{(\vec{\kappa}_M \cdot \vec{\kappa}_M - \Delta_1 + i0^+) ((\vec{q}_M + \vec{\kappa}_M) \cdot (\vec{q}_M + \vec{\kappa}_M) - \Delta_2 + i0^+)} \quad (58)$$

where

$$\Delta_1 = n^2 + \xi_1 a^2 \tag{59}$$

$$\Delta_2 = (n + \ell)^2 + \xi_2 a^2 \tag{60}$$

and, as in (8), dot products in (58) are Minkowski [see Eq. (9)]. As discussed in Section 2, the right-hand side of (58) is in a form suitable for numerical evaluation with pySecDec. As for $\tilde{\Pi}_0$ in (54), its equivalent integral in terms of Minkowski-space propagators (in $D = 4 - 2\epsilon$ dimensions) is

$$\tilde{\Pi}_0(q, \xi_i) = \frac{1}{2} \int \frac{d^D \kappa}{(2\pi)^D} \frac{1}{(\kappa^2 - \xi_1 a^2 + i0^+) ((\kappa + q)^2 - \xi_2 a^2 + i0^+)} \tag{61}$$

where

$$\kappa^0 = i\kappa_E^0 \text{ and } q^0 = i\ell. \tag{62}$$

The right-hand side of (61) is also in a form suitable for numerical calculation using pySecDec.

Before proceeding with some numerical results for the finite-temperature correction two-point function Π_s , we summarize some key aspects associated with the pySecDec evaluation of (53). First, analytic methods have been used to regulate the divergences in the finite-temperature Matsubara sum (42), and it has been demonstrated that these divergences cancel against the divergent zero-temperature result. As for the three-point function, these analytic methods also improve the numerical convergence of the Matsubara sum. Second, it should be verified that the pySecDec-computed values of (58) appearing in the sum are finite, and that the divergent part of (61) as computed with pySecDec is $1/(32\pi^2\epsilon)$ as needed to cancel the divergences. Finally, we also note that in (53), there is a natural cancellation of the γ_E and $\log(4\pi)$ as shown analytically in (52).

As an example of results obtained from the procedure described above for numerically calculating Π_s , we plot Π_s as a function of a at $\vec{q} = 0$ for several values of ℓ in Figure 8. Also, in Figure 9, we plot Π_s as a function of q^1 where $\vec{q} = (q^1, 0, 0)$ at $\ell = 1$ for several values of a . In obtaining these plots, it has been verified that the case where $\ell = 0$ and $\vec{q} = 0$ agrees with the results of Ref. [1] given in a considerably different form and approach, providing a robust validation of the regularization method used for the Matsubara sum. In obtaining Figure 8 we have also compared the pySecDec numerical results with an analytic version of our calculation that is possible in the limiting case $\xi_1 = \xi_2 = 1$ and $\vec{q} = 0$. Within the remaining $\{a, \ell\}$ parameter space, the difference between the analytic and pySecDec numerical results are smaller than the pySecDec-provided numerical errors, providing a validation of the methodology. As for the three-point function, the advantages and adaptability of our finite temperature numerical pySecDec methodology are illustrated by the incredible diversity of physical scales (mass, temperature, momentum) encompassed by Figures 8–9.

4 Discussion

In this paper we have developed methods to enable application of pySecDec [16,17] to numerically evaluate dimensionally-regulated, finite-temperature bosonic loop integrals in the imaginary time (Matsubara) formalism. The methods are developed at one-loop order in four spacetime dimensions and consist of two main elements. The first element is an inverse Wick rotation of a spatial component that maps a finite-temperature spatial integral into a form that enables the use of pySecDec. This inverse Wick rotation is a generic methodology that can easily be extended to higher-loop integrals, various loop topologies, and to different choices of spacetime dimension. The second methodological element develops asymptotic forms that can be used to regulate and accelerate convergence of the Matsubara sum. In principle, this asymptotic methodology could be extended to higher-loop calculations, but, of

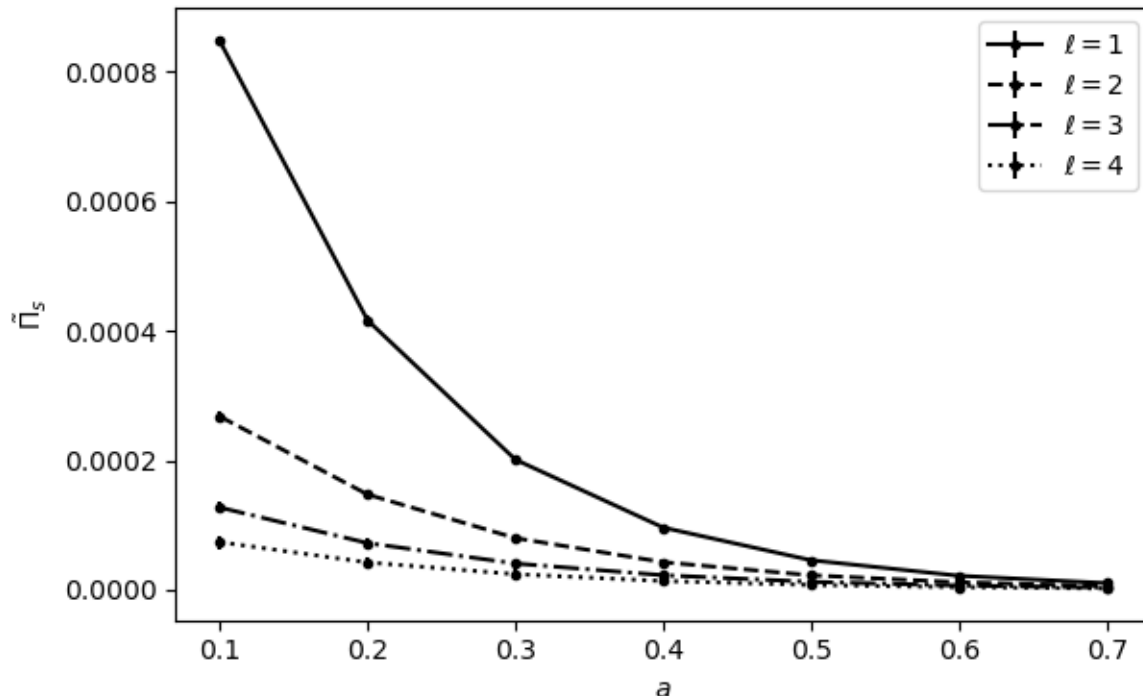


Figure 8: The dimensionless, finite-temperature 2-point function correction Π_s versus a for $\xi_1 = \xi_2 = 1$ and $\vec{q} = 0$ at various values of ℓ . Error bars (where visible) reflect the numerical uncertainty as determined by pySecDec.

course, the analysis would become increasingly complicated with multiple Matsubara sums. Both of the methodological elements are easily adaptable to fermionic finite-temperature loop integrals.

Two examples were used to develop and illustrate our finite-temperature pySecDec methodology. The finite-temperature bosonic three-point function was first considered because in four spacetime dimensions, the loop integrals and Matsubara sum converge. However, although dimensional regularization is not strictly needed, we find that pySecDec still provides demonstrable advantages in computational efficiency compared with direct numerical integration using standard Python functions such as `tplquad` from `scipy.integrate` or Mathematica's `NIntegrate`. We thus conclude that pySecDec is particularly well optimized to loop integrals, and is capable of handling the full diversity of scales that could occur in a finite-temperature system. Despite this numerical efficiency, we also demonstrated that convergence of the Matsubara sum can be accelerated by using analytic methods for the asymptotic form of the finite-temperature series.

The second example of the finite-temperature bosonic two-point function in four spacetime dimensions has an additional complication of divergences in the Matsubara sum that we regulate using dimensional regularization combined with the asymptotic form of the finite-temperature series. We demonstrate that this divergence is identical to that of the zero-temperature two-point function, and hence the finite-temperature correction (48) is finite as expected. An algorithm was presented for applying pySecDec to the two-point finite-temperature correction by combining analytic methods and extracting specific portions of the zero-temperature loop integral in pySecDec. In the analysis of the two-point function, the numerical pySecDec results for the finite-temperature correction were compared against known results [1] in specific limiting cases.

In the various figures (see Figures 2–6 and Figures 8–9) used to demonstrate our pySecDec finite-temperature loop-integral methodology, we have shown the numerical uncertainties reported by pySecDec. In obtaining these figures, we have tested the pySecDec results against limiting cases where we

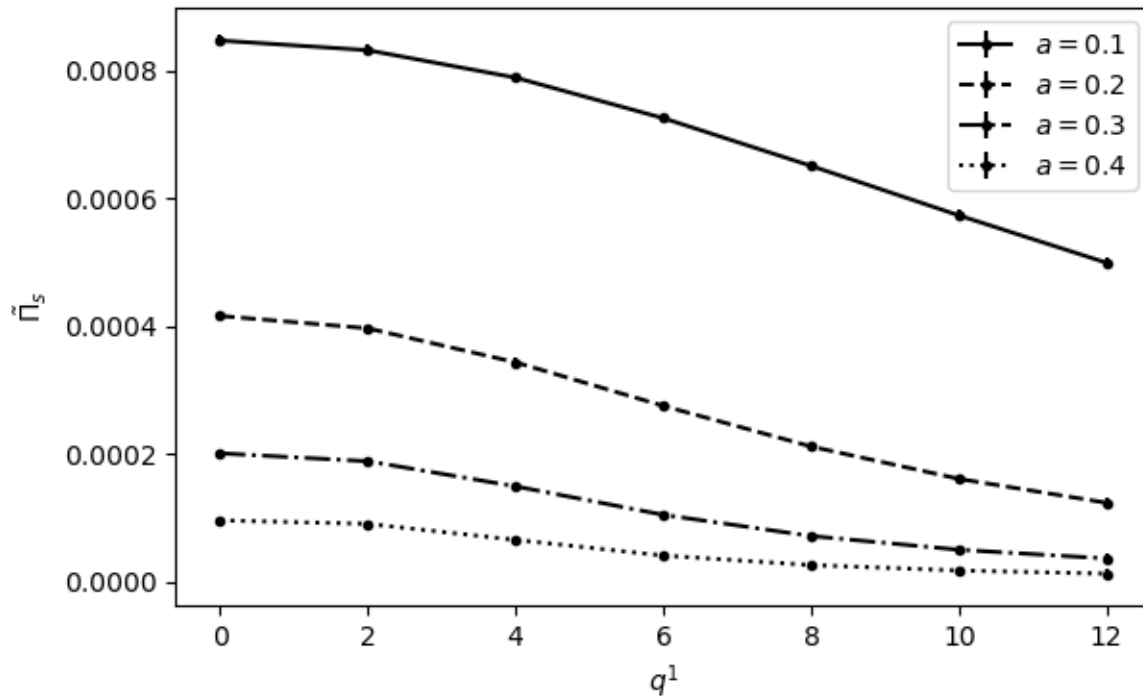


Figure 9: The dimensionless, finite-temperature 2-point function correction Π_s versus q^1 where $\vec{q} = (q^1, 0, 0)$ for $\xi_1 = \xi_2 = 1$ and $\ell = 1$ at various values of a . Error bars (where visible) reflect the numerical uncertainty as determined by pySecDec.

can perform analytic calculations, and find the difference between the analytic and pySecDec numerical results are smaller than the pySecDec-provided numerical errors, and see no evidence of numerical noise in the data generated by pySecDec.

Acknowledgments

TGS and DH are grateful for research funding from the Natural Sciences & Engineering Research Council of Canada (NSERC).

References

- [1] A. Das, “Finite Temperature Field Theory”, (World Scientific, 1997).
- [2] M. Laine and A. Vuorinen, “Basics of Thermal Field Theory,” Lect. Notes Phys. **925** (2016) 1, (Springer, 2016), [arXiv:1701.01554 [hep-ph]].
- [3] J.I. Kaputsa, C. Gale, “Finite-Temperature Field Theory: Principles and Applications”, (Cambridge U. Press, 2006).
- [4] A. Ayala, C. A. Dominguez and M. Loewe, Adv. High Energy Phys. **2017** (2017) 9291623, [arXiv:1608.04284 [hep-ph]].
- [5] G. Aarts, J. Aichelin, C. Allton, A. Athenodorou, D. Bachtis, C. Bonanno, N. Brambilla, E. Bratkovskaya, M. Bruno and M. Caselle, *et al.* Prog. Part. Nucl. Phys. **133** (2023) 104070 [arXiv:2301.04382 [hep-lat]].

- [6] M. Quiros, [arXiv:hep-ph/9901312 [hep-ph]].
- [7] D. Croon, [arXiv:2307.00068 [hep-ph]].
- [8] P. Athron, C. Balázs, A. Fowlie, L. Morris and L. Wu, [arXiv:2305.02357 [hep-ph]].
- [9] M. E. Carrington, Phys. Rev. D **45** (1992) 2933–2944.
- [10] J. R. Espinosa, M. Quiros and F. Zwirner, Phys. Lett. B **314** (1993) 206–216, [arXiv:hep-ph/9212248 [hep-ph]].
- [11] J. R. Espinosa, T. Konstandin and F. Riva, Nucl. Phys. B **854** (2012) 592–630, [arXiv:1107.5441 [hep-ph]].
- [12] W. C. Huang, F. Sannino and Z. W. Wang, Phys. Rev. D **102** (2020) 095025, [arXiv:2004.02332 [hep-ph]].
- [13] D. E. Morrissey and M. J. Ramsey-Musolf, New J. Phys. **14** (2012) 125003, [arXiv:1206.2942 [hep-ph]].
- [14] C. Caprini, M. Chala, G. C. Dorsch, M. Hindmarsh, S. J. Huber, T. Konstandin, J. Kozaczuk, G. Nardini, J. M. No and K. Rummukainen, *et al.* JCAP **03** (2020) 024, [arXiv:1910.13125 [astro-ph.CO]].
- [15] T. Matsubara, Prog. Theor. Phys. **14** (1955) 351–378.
- [16] S. Borowka, G. Heinrich, S. Jahn, S. P. Jones, M. Kerner, J. Schlenk and T. Zirke, Comput. Phys. Commun. **222** (2018) 313–326, [arXiv:1703.09692 [hep-ph]].
- [17] G. Heinrich, S. P. Jones, M. Kerner, V. Magerya, A. Olsson and J. Schlenk, Comput. Phys. Commun. **295** (2024), 108956 [arXiv:2305.19768 [hep-ph]].
- [18] G. Heinrich, Int. J. Mod. Phys. A **23** (2008) 1457–1486, [arXiv:0803.4177 [hep-ph]].
- [19] J. A. M. Vermaseren, [arXiv:math-ph/0010025 [math-ph]].
- [20] J. Kuipers, T. Ueda and J. A. M. Vermaseren, Comput. Phys. Commun. **189**, 1-19 (2015) doi:10.1016/j.cpc.2014.08.008 [arXiv:1310.7007 [cs.SC]].
- [21] B. Ruijl, T. Ueda and J. Vermaseren, [arXiv:1707.06453 [hep-ph]].
- [22] M. Galassi, J. Davies, J. Theiler, B. Gough, G. Jungman, P. Alken, M. Booth and F. Rossi, “GNU Scientific Library Reference Manual, 3 ed.” (Network Theory Ltd., 2009).
- [23] T. Hahn, Comput. Phys. Commun. **168** 78–95 (2005), [arXiv:hep-ph/0404043 [hep-ph]].
- [24] T. Hahn, J. Phys. Conf. Ser. **608** (2015) 012066, [arXiv:1408.6373 [physics.comp-ph]].
- [25] S. Esau and D. Harnett, Eur. Phys. J. A **55** (2019) 31, [arXiv:1806.00157 [hep-ph]].
- [26] K. Ray, D. Harnett and T. G. Steele, Phys. Rev. D **108** (2023) 034001, [arXiv:2211.00155 [hep-ph]].
- [27] P. Pascual and R. Tarrach, “QCD: Renormalization for the Practitioner”, Lecture Notes in Physics v. 194 (Springer, 1984).